Adaptive Spatial Lattice Manufacturing (ASLM): A novel approach to efficient lattice structure production

Justin Dirrenberger, Pierre Lapouge, Rachel Azulay, Peter Evers, Tom Vroemen

Materials & Design 249 (2025) 113553

Contents lists available at ScienceDirect

Materials & Design

journal homepage: www.elsevier.com/locate/matdes

Adaptive Spatial Lattice Manufacturing (ASLM): A novel approach to efficient lattice structure production

Justin Dirrenberger [a,b,c,*], Pierre Lapouge [b], Rachel Azulay [b], Peter Evers [b], Tom Vroemen [b]

[a] PIMM, Arts et Métiers, Cnam, CNRS UMR 8006, 151 bd de l'Hôpital, 75013 Paris, France
[b] TETMET, 1 parvis de la Défense, 92060 Paris–La Défense, France
[c] Institut universitaire de France (IUF), France

ARTICLE INFO

Keywords:
Additive manufacturing
Lattice structures
Laser welding
Architectured materials
Processing
Adaptive Spatial Lattice Manufacturing
ASLM
Robotics
Automation

ABSTRACT

Adaptive Spatial Lattice Manufacturing (ASLM) represents a groundbreaking method for fabricating lattice structures by leveraging AI-driven robotic laser welding. Unlike traditional additive manufacturing techniques, ASLM corresponds to a direct assembly of solid rods, by welding, offering remarkable benefits in energy efficiency, dimensional accuracy, and scalability. This paper introduces the ASLM process, detailing its computational design principles, build mechanics, and material compatibility using AISI 316L stainless steel. Through mechanical characterization and finite element analysis, the structural performance of ASLM-produced lattices was evaluated, highlighting the predictability and reliability of their mechanical properties. Key findings demonstrate ASLM's capability to address critical limitations of conventional additive manufacturing methods, such L-PBF, LMD or EBM, while producing robust, scalable, and efficient designs. Challenges, including localized heat-affected zones and internal stress management, are also discussed, along with future prospects for multi-material integration and industrial applications in aerospace, construction, and beyond. ASLM establishes a transformative path for lattice manufacturing and advances the integration of architectured materials in diverse engineering domains.

1. Introduction

Architectured materials represent a significant improvement over traditional materials due to their optimized microstructures which yield superior properties [1–3]. As a subset of architectured materials, lattice structures, known for their optimal geometric configurations, provide exceptional mechanical performance while minimizing the use of materials [4–6]. These structures have garnered significant attention across various engineering fields due to their lightweight nature and remarkable specific mechanical properties such as strength-to-weight or stiffness-to-weight ratios [7–10]. Lattice structures are also appreciated for their highly tailorable anisotropic behavior [11,12], and their ability to act as effective metamaterials [13–19].

The evolution of additive manufacturing technologies has played a crucial role in the advancement of lattice materials, enabling more complex designs and improving structural capabilities [20–23]. However, the full industrial integration of lattice structures has been impeded by several challenges inherent to conventional additive manufacturing methods such as Laser Powder Bed Fusion (L-PBF), Laser Metal Deposition (LMD) and Electron Beam Melting (EBM). These include high energy consumption, limited material availability, scalability issues, and environmental concerns [24–29]. In addition to these challenges, many obstacles stand against the use of lattice structures obtained through additive manufacturing (AM) within the industrial world: buckled or collapsed struts for slender lattice structures due to recoater influence during L-PBF, or thermal strain incompatibility [30,31]; surface defects/roughness being a source of asymmetry and buckling [32,33]; scalability for large scale production [34]; dimensional inaccuracies [35,36]; deviation of strut shape due to thermally induced stresses [37]; particles adhesion [36]; staircase effect [38]; porosity induced by inappropriate process parameters [39,40].

Based upon an understanding of all the aforementioned limitations identified in the literature, the purpose of the present paper is to introduce the concept, coined by the authors, of Adaptive Spatial Lattice Manufacturing (ASLM), which emerges as a revolutionary alternative to traditional AM. This innovative process combines AI-driven robotics and accurate laser spot welding for solid-rod assembly. ASLM is not a classical AM process, in the sense that no material is being extruded, or deposited layer-by-layer or voxel-by-voxel, but rather a direct assembly process for efficiently manufacturing lattice structures, with solid

* Corresponding author at: PIMM, Arts et Métiers, Cnam, CNRS UMR 8006, 151 bd de l'Hôpital, 75013 Paris, France.
E-mail address: justin.dirrenberger@ensam.eu (J. Dirrenberger).

https://doi.org/10.1016/j.matdes.2024.113553
Received 22 October 2024; Received in revised form 5 December 2024; Accepted 16 December 2024

Available online 19 December 2024

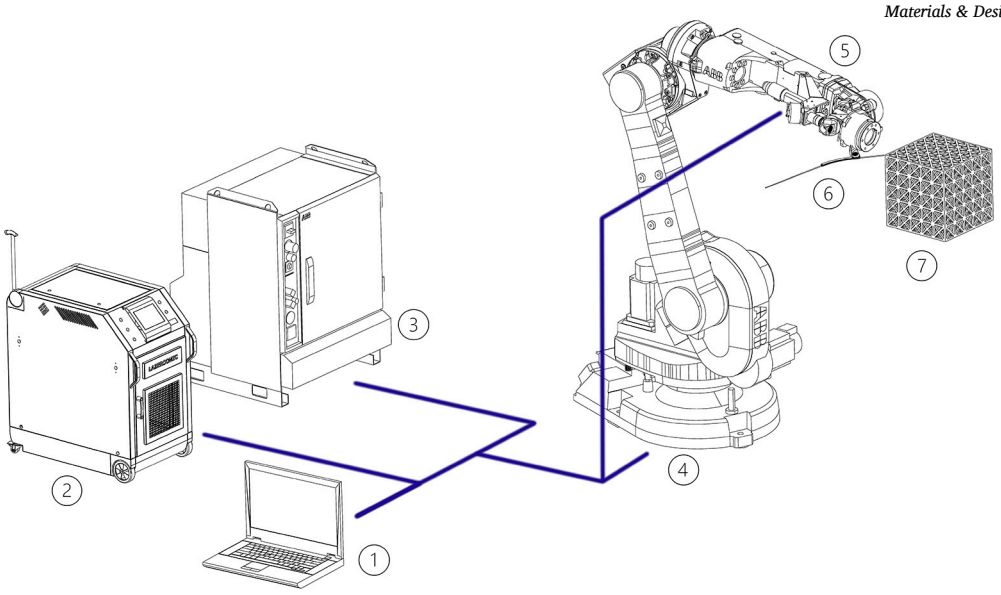

Fig. 1. Schematic of the ASLM process: 1. System control; 2. Laser source; 3. Robot controller; 4. 6-axis robot; 5. Laser beam steering; 6. Wire holder; 7. ASLM-produced structure.

rods being cut and welded together. In ASLM, the term *Adaptive* refers to the variable rod length, which is the counterpart of the *Non-adaptive* voxel size in traditional AM. *Spatial* refers to three-dimensional nature of the structures being manufactured using this technology, i.e. *Lattices*. The term *Adaptive* really characterizes ASLM in comparison to other AM processes, as the variable length of each building unit is a major difference compared to traditional AM in which voxels are used with a fixed size, mainly due to the CAD slicing step and building path generation. This does not mean that AM cannot produce lattices, it just means that the fixed voxel resolution is slowing down the process very much, compared to a variable rod length.

This study aims to formally introduce ASLM technology to the scientific community, providing new insights into advancements in manufacturing and design through the integration of computational methods and fully automated fabrication processes.

This paper is organized as follows. First, the design and processing chain is described. In Section 3 the material considered for validating the process is presented. Mechanical characterization and finite element simulation of ASLM-produced structural samples are made in Section 4. The results obtained in this work are discussed in Section 5 along with the challenges facing ASLM. Finally, in Section 6 concluding and prospective remarks are drawn.

2. ASLM technology

2.1. Process description

ASLM is an innovative manufacturing process that consists in assembling rods in any direction using laser spot welding. The rods can be made of any weldable material, e.g. metals or thermoplastic polymers. As shown in Fig. 1, an ASLM production unit is composed of a few elements: system control, laser source, robot controller, 6-axis robot, laser beam steering, wire holder, possibly a gas supply system (not depicted) and image acquisition equipment. In this paper, the process is illustrated with an ABB IRB1660ID 6-axis robot; nevertheless, a gantry or linear actuators could be used instead.

The robot positions the rod at its predetermined location in the structure to be built. The focused laser beam welds it at one end and cuts it at the other end. The cut is obtained by melting the cross-section of the rod at the cut point with the laser and pulling on it with a robot motion before it solidifies. Therefore, no additional actuator is required to pull or push on the rod. In the following, the rod is mounted on the robot head through a slightly curved tube that holds the rod by contact friction, that is, the wire holder depicted in Fig. 1. The friction is just high enough for the wire to be held in place when the holder is vertical. As the robot moves along the wire direction from the weld to the end to be cut, the newly created rod tip remains close to its original position, i.e. before the weld-and-cut operation. There is some local geometrical variability induced by the ASLM process due to the unpredictable nature of laser spot welding. The shape of the molten material drop during the welding process differs from one weld to the next, therefore introducing some randomness at the nodes. In ASLM, if the defect is deemed critical, then the weld will be rejected and the process will restart with a new weld cycle. Overall these local variabilities are compensated for over the whole structure, yielding accurate dimensions for final parts.

Beam steering is achieved using two piezoelectric actuators that reorient a dichroic mirror in two directions. The range of laser beam steering is of a few millimeters around the tip of the rod. A camera is placed on the other side of the mirror, providing a view of the area around the rod tip. This camera makes it possible to ensure that the rod is in contact with the structure and the weld point to be placed at the interface between the two. In the version of ASLM presented in this paper, three more cameras are mounted on the robot head. These cameras capture images from different angles to ensure the position of the tip at the junction with the structure and assess the quality of the weld. If an offset is detected between the rod position and the rest of the structure, the controller can adjust the position of the tip to match the expected position. This adjustment is performed automatically by a trained machine learning model capable of accurately segmenting the rod tip and the structure node. In the event of an unsatisfactory weld, the controller raises an alarm for an operator to physically remove the rod from the structure. This last operation could be automated in the future. As of 2024, image segmentation, monitoring, decision making, as well as subsequent process automation such as welding is operated through an internally developed AI tool based off Meta's SAM-2 [41].

2.2. Computational design

Generating geometries for ASLM has to be done following specific requirements, coming from both the processing constraints, e.g. rod diameter, nodal connectivity, etc., and the functional properties of the produced part, e.g. stiffness, strength, thermal conductivity, etc. Both types of constraints must be considered in a synergistic manner at three different scales: the rod scale, the assembly path scale, and the global

Table 1
Chemical composition (wt %) of the AISI 316L wire.

C	Mn	Si	P	S	Cr	Ni	Cu	N	Mo
0.019	1.720	0.340	0.028	0.004	18.700	11.170	0.380	0.075	2.570

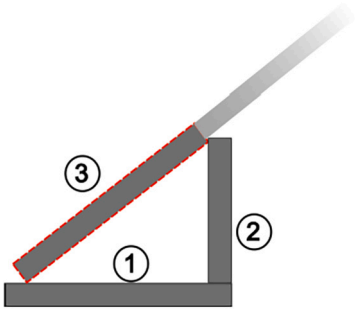

Fig. 2. Drawing of the build assembly for 3 rods. The numbers indicate the build order for the rods. The second rod is cut shorter to fit in the wire for the third rod.

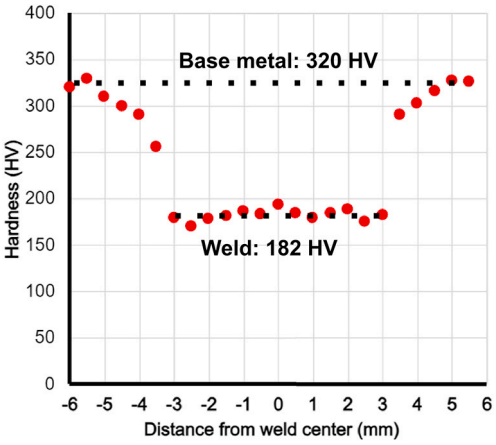

Fig. 3. Vickers hardness measurement of the weld cross section.

scale. In the present work, the processing constraints consist mainly in ensuring the alignment of rods while being assembled with the rest of the structure. Functional requirements depend mostly on the properties of the rod constitutive material and the structural geometry of the lattice at the local and global scales for effective mechanical properties, as well as other geometrically induced properties such as damping, wave guiding, actuation, etc. Various approaches can be adopted to generate the robotic assembly path. Unlike conventional additive manufacturing, one cannot rely on 3D-to-2D slicing software to generate the overall structure and its assembly sequence for ASLM. Hence, the first step consists of discretizing the 3D volume into a mesh, e.g. a tetrahedral finite element mesh. This mesh can then be optimized by a specific algorithm to fulfill requirements regarding both processing constraints and functional properties, e.g. genetic algorithm-based multi-objective truss topology optimization [42,43].

2.3. Build process

The uncut rods are inserted into the structure one at a time. It is noteworthy that the process could be extended to other building units, such as tubes, plates, or any arbitrary shape, given that an assembly path for such unit shapes can be determined. There must be enough space at every step for the new rod to fit in. Different strategies and methods can be used to avoid this problem: cutting the rods shorter, offsetting the rods in specific directions, and building the new rods on top of the previous ones. The authors favored cutting the rods shorter, as it preserves the geometry of the desired lattice structure, as depicted in Fig. 2.

The updated rod length can be deduced from basic trigonometry. A rod is shortened until it is tangent with a rod fed afterwards at the same node. The required length is thus determined by the smallest angle formed by the current rod and a subsequent contiguous rod.

To avoid collision between the robot and the structure being built, it is necessary to define an appropriate build direction and associated rod orientations. As the robot can build rods at any angle, there is no major limitation on the build direction. In particular, unlike most 3D printing technologies, the ASLM process has no restriction on overhang angles. For convenience, the build direction is chosen from the bottom of the structure towards the top. A secondary build direction can be selected to build the part from left to right or from the inside out. The rod orientation is then derived as the opposite to the build direction. The build direction also defines the build order of each rod.

Theoretically, any structure discretized in the form of solid rods can be manufactured using ASLM. Nevertheless, anchor points are necessary to hold the structure during the building process. At the start of a build, an anchor point is placed at the location of the minimal global height within the structure. The first rod can then be welded to this anchor point and the build continues step-by-step, by welding the new rods to the existing ones according to the predetermined build order. New anchor points can be placed to support local minima or sharp corners, e.g., to avoid warping after welding.

3. Materials characterization

In order to demonstrate the feasibility of the process, a 1.6 mm thick AISI 316L stainless steel wire was selected. This material was chosen as previous studies had demonstrated its excellent mechanical properties [44] and excellent weldability due to its low carbon content [45,46]. The wires are supplied as 1 m long straight rods, commonly used for manual TIG welding. The material composition of the wire is given in Table 1.

Two pieces of 2.5 cm long wires were welded together vertically by the robot with a laser power of 500 W emitted for a duration of 0.3 s. A gas nozzle delivered a constant argon flow rate at 16 l/min on the top of the weld before and after the laser shot. These parameters are representative of the parameters used during a build. The welded wires were then cut along their length and polished at different grits until mirror finish. The samples were then etched with an A3 electrolyte solution from Struers to reveal the grain structure [47]. Microstructural observation was performed by both optical microscopy using an Axio Imager A1M (Zeiss, Germany) and scanning electron microscopy on an EVO MA-10 (Zeiss, Germany). Hardness was measured every 500 μm at a constant load of 0.3 N using a MHT hardness tester (CSM Instruments, Switzerland) with a Vickers indent tip, following the ASTM E2546-15/ISO 14577-1 recommendation.

The hardness measurements are compiled in Fig. 3. The base material exhibits a hardness of 320 HV, typical of a plastically hardened sample [48], as expected from a wire produced by drawing. In the welded area, the hardness decreases by 43% to 182 HV. Although lower, this hardness value remains close to what is commonly measured for AISI 316L samples [49]. A heat-affected zone (HAZ) of two millimeters is present on each side of the weld with a sharp transition towards the base metal.

Fig. 4 shows the microstructure of both the base metal and the welded section. The base metal (wire) exhibits a mix of equiaxial morphology, and grains stretched along the rolling direction. The welded

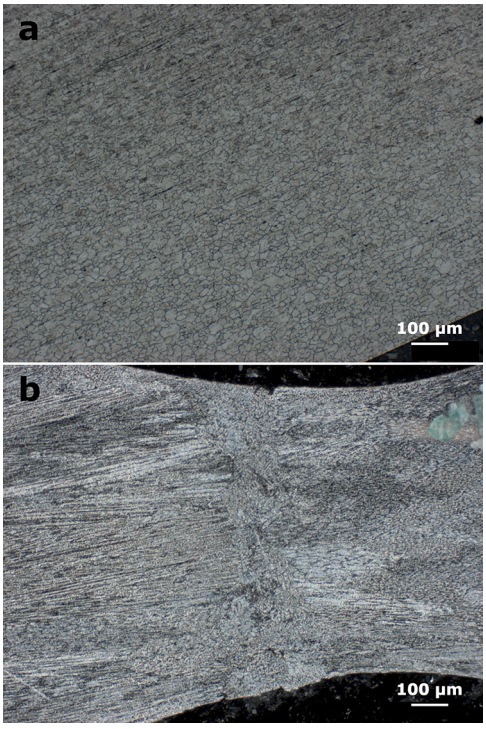

Fig. 4. Microstructure of (a) the base metal, (b) the welded section.

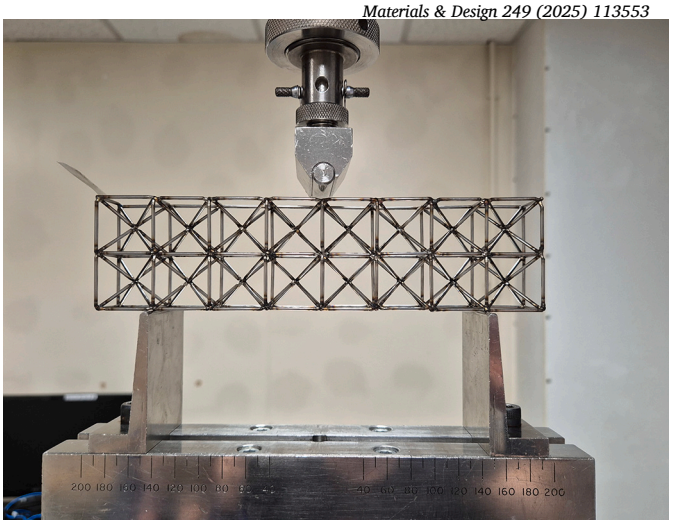

Fig. 5. Experimental setup for 3-point bending on a BCC+SC sample.

Table 2
Parameters for the constitutive AISI 316L wire materials.

Young's modulus (GPa)	Poisson's ratio -	Yield strength (MPa)	Ultimate tensile strength (MPa)
210	0.3	410	600

section exhibits dendritic grain growth parallel to the wire, which indicates a solidification front mostly normal to the wire cross-section. In the center of the weld area, where the solidification fronts from both sides meet, a more distorted microstructure can be found with dendrites mostly normal to the wire cross-section.

Scanning electron microscopy was used to determine porosity in both pristine and welded samples. The weld area presents a slight increase of porosity (0.7%) with microbubbles (≤ 1 µm) trapped in the matrix. For the sake of brevity, the micrographs are not presented here.

4. Structural performance

Large-scale samples are produced by ASLM for evaluating their mechanical performance. In this study, they are made of AISI 316L stainless steel. Each sample measured 8x2x1 unit cells, with each unit cell having dimensions of 25x25x25 mm. The actual dimensions of the samples were measured to be 200.0x50.0x25.0 mm with a precision of ±0.5 mm, yielding a dimensional accuracy below 0.5%. For a larger sample, the accuracy would be even better; this is made possible by the positioning compensation feature previously introduced in Section 2.1. Three distinct unit cell geometries were tested: Simple Cubic (SC), Body-Centered Cubic + Simple Cubic (BCC+SC), and Face-Centered Cubic + Simple Cubic (FCC+SC), resulting in a total of nine samples (three per unit cell type).

The samples were subjected to three-point bending tests. The span between the supports was 150 mm and the linear load was applied through the thickness in the middle of the upper face of the structure, as shown in Fig. 5. The samples were oriented so that the thickness would be larger than the width, in order for the beam to be loaded in its stiffer plane, to generate higher stresses in the structure and possibly reach for failure. This test is based on the ASTM D7249 norm.

The load-displacement curves for both experiment and simulation are available as Supplementary Material. As shown on the curves, the simulation and experiments exhibit consistent trends in terms of deformation mechanisms, peak and stabilized load values. The discrepancies in terms of stiffness mainly come from the fact that no strain gauge was used for measuring the actual displacement and strain of the sample, making the exploitation of experimental curves for stiffness spurious. The SC sample exhibited a global deformation response, where the entire sample was deformed. The measured behavior is typical of a softening elastoplastic response, exhibiting no peak force. The BCC+SC and FCC+SC samples produced a different response, caused by local deformation due to plastic buckling of the beams within the unit cells. This elastoplastic behavior is characterized by a peak force followed by a drop in stiffness due to the local plastic buckling, finally a stabilization is reached. The FCC+SC sample reached a peak load of 3.7 kN, stabilizing at approximately 1.7 kN. The BCC+SC sample had a lower peak load of 2.6 kN, with stabilization occurring around 1.5 kN. In both cases, the failure was due to buckling and not fracture at the weld points. To the knowledge of the authors, as of 2024 there is no data available in the literature about mechanical performance of similar lattice structures –in terms of sample dimensions, loading conditions and volume fraction– produced by additive manufacturing, e.g. L-PBF, EBM, etc. Therefore no direct mechanical performance comparison could be made, except for the finite element simulations presented hereafter.

Numerical simulations were performed using the finite element method through ANSYS Mechanical with implicit quasi-static structural analysis using volumic tetrahedral quadratic elements (C3D10). The simulations incorporated the material properties of AISI 316L, using an elastoplastic behavior with linear isotropic hardening and material parameters given in Table 2, taken from the technical sheet provided by the material supplier (Sadevinox, France). Damage modeling was not considered in the simulation.

A displacement was applied at the top of the sample, while one end was fixed at the bottom, and the other was constrained to prevent out-of-plane and in-height displacements. The simulations predicted a global deformation behavior for the SC sample, consistent with the experimental results. For the BCC+SC and FCC+SC samples, the simulations also captured the localized buckling mode. The FCC+SC sample reached a peak load of 3.9 kN, stabilizing at 1.7 kN, while the BCC sample peaked at 2.6 kN and stabilized around 1.2 kN. Bending stiffness was computed in the simulations. The simulation took from 13 minutes for the SC structure (with 658209 elements) to 33 minutes for the BCC+SC structure (with 1283703 elements) using Ansys Mechanical on a workstation

Table 3
Results for experimental and computational 3-point bending.

Unit-cell	Theoretical mass (g)	Sample mass (g)	Peak load simulation (N)	Peak load experiment (N)	Stiffness ($N.m^{-1}$)
SC	42.32	42.22	-	-	1.05×10^5
BCC+SC	83.69	81.67	2647	2576	6.58×10^6
FCC+SC	118.23	114.78	3918	3672	9.68×10^6

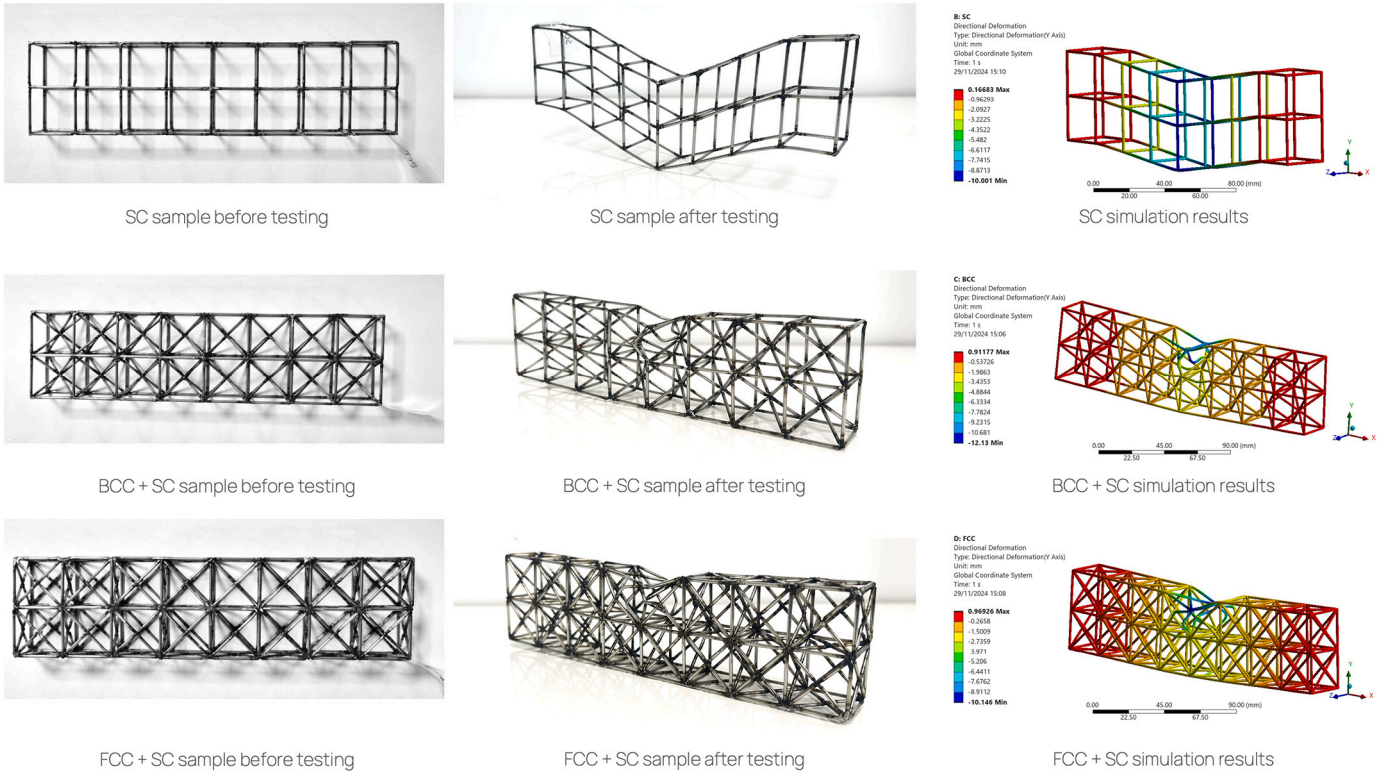

Fig. 6. Comparison between experimental and simulated 3-point bending test on samples for SC, BCC+SC and FCC+SC.

equipped with an Intel Xeon W5-2455X CPU. The results of both experiments and simulations are gathered in Table 3.

When comparing the experimental results with the simulations, the overall trends in the deformation and plastic failure mechanisms were consistent across both. The finite element analysis overestimates the response of the lattice structures, as one would expect from simulation without defects and damage. Nevertheless, the overall response of the structure is consistent with the experiments as the behavior of a lattice structure, albeit showing minor local geometrical defects, as can be seen in Fig. 5, is mainly driven by its topology, i.e. its mesoscopic geometrical arrangement. The SC samples in both cases showed global deformation, while the BCC+SC and FCC+SC samples showed local buckling. The peak loads and post-peak stabilization values for the BCC+SC and FCC+SC samples were slightly higher in the simulations compared to the experimental results. The failure modes and general elastoplastic response remained aligned between experimental and numerical results (Fig. 6).

5. Discussion

This study's findings emphasize the substantial potential of ASLM in fabricating lattice structures. ASLM overcomes many inherent limitations of conventional additive manufacturing techniques like L-PBF and EBM, particularly in terms of energy efficiency, precision, and scalability. By leveraging AI-driven robotic laser welding, ASLM enables precise assembly with minimal material waste, and its ability to directly weld and cut rods enhances overall efficiency. The three-point bending tests revealed that FCC+SC and BCC+SC structures exhibit predictable buckling behavior under load, with consistent results across both experimental tests and numerical simulations. This consistency indicates that ASLM can produce highly reliable lattice structures whose mechanical properties can be accurately predicted through computational modeling. Additionally, ASLM effectively mitigates common defects such as surface roughness, porosity, and dimensional inaccuracies—issues frequently encountered in additive manufacturing processes. The combination of robotic assembly and machine learning-driven precision adjustments ensures high-quality welds and reduces the likelihood of manufacturing errors that could compromise structural integrity. However, ASLM is not without challenges. One key limitation is the potential for localized HAZ in the welds, which, as hardness measurements show, may result in decreased mechanical strength in those areas. Although the HAZ is relatively small and does not significantly impact the structure's overall performance, further research is needed to mitigate this effect. Another challenge resides in the internal stresses induced by the thermal expansion taking place during the welding process. If not taken into account during the design process, these internal thermo-mechanical stresses might end up in premature buckling or dimensional inaccuracies. Moreover, while the process shows promise for scaling up, practical industrial implementation may require additional optimization of the robotic system to handle larger and more complex structures. The adaptability of ASLM for different material types, such as metals and thermoplastic polymers, opens up a wide range of potential appli-

cations across various industries, including aerospace, automotive, and biomedical sectors. Particularly noteworthy is ASLM's potential for in-orbit manufacturing, where its energy efficiency and precision could make it an ideal candidate for constructing structures in space environments. Short-term developments for ASLM include the capability to produce lattice structures with multiple materials or wire thicknesses, as well as various wire cross-sections like tubular or prismatic shapes. As of 2024, a major limitation of ASLM is the minimal length of rods to be considered for manufacturing; as a matter of fact the economic and environmental efficiency of ASLM is related to the availability of weldable wire such as 1-2 mm diameter metal wire. Working with 1.0 mm diameter entails that the minimal length of unit-rod would be of at least a few millimeters. The availability of significantly thinner wire is more difficult and would probably yield several order of magnitude in terms of material cost that would negatively impact the efficiency of ASLM. Another limitation is that the ASLM technology is intended to be used on thick rods (from 10 mm diameter and up) as it would likely create processing difficulties, but more importantly because it would be preferable to replace a thick rod by an equivalent truss beam made of thinner rods, a solution that is enabled by ASLM. For industrial implementation, adding a linear actuator to the ASLM production unit could enable continuous building strategies with an infinite build range. Other scenarios might involve on-site ASLM production in the construction sector or part repair in industries like defense. In summary, ASLM offers a promising alternative to traditional additive manufacturing techniques, with the potential to foster lattice structure production. Continued development to address challenges such as localized heat effects and improved scalability will be crucial for the broader adoption of ASLM in industrial applications.

6. Conclusions and perspectives

Limitations of existing AM processes have been reviewed and a novel process has been introduced accordingly in this paper.

The development of ASLM represents a paradigm shift in the production of lattice structures, overcoming many limitations inherent to conventional AM techniques. By leveraging AI-driven robotics and precise laser welding, ASLM achieves enhanced scalability, energy efficiency, and dimensional accuracy, distinguishing itself as a transformative alternative to methods such as L-PBF, EBM or LMD.

Through the demonstration of ASLM using AISI 316L stainless steel, this study highlights the robustness and versatility of the process. Mechanical testing of ASLM-produced structures revealed consistent and predictable performance, validated by finite element analysis. These results emphasize ASLM's ability to deliver reliable and precise structures with superior mechanical properties, even in scenarios that typically challenge traditional AM methods.

Despite its advantages, ASLM faces challenges such as localized heat-affected zones and internal stresses that could impact structural integrity if not properly managed. Addressing these issues, along with refining the scalability and material versatility of the technology, will be crucial for its adoption in industrial applications. Nevertheless, the potential for multi-material integration and applicability across diverse industries—including aerospace, construction, and biomedical engineering—underscores its broad utility.

In conclusion, ASLM establishes itself as a disruptive innovation in lattice structure manufacturing, bridging the gap between advanced material design and industrial scalability. Continued research and development will further refine the process, enabling its integration into a wide array of engineering applications, ultimately fostering the adoption of architectured materials.

Further on-going work includes full life-cycle analysis of case-specific parts being produced using ASLM, as well as expanding the range of materials used for the welded rods.

CRediT authorship contribution statement

Justin Dirrenberger: Writing – review & editing, Writing – original draft, Supervision, Methodology, Investigation, Funding acquisition, Conceptualization. **Pierre Lapouge:** Writing – review & editing, Writing – original draft, Methodology, Investigation. **Rachel Azulay:** Writing – review & editing, Writing – original draft, Methodology, Investigation. **Peter Evers:** Writing – review & editing, Writing – original draft, Supervision, Software. **Tom Vroemen:** Writing – review & editing, Writing – original draft, Supervision, Conceptualization.

Declaration of competing interest

The authors declare that they have no known competing financial interests or personal relationships that could have appeared to influence the work reported in this paper.

Acknowledgements

The authors would like to gratefully acknowledge Bpifrance for early financial support through its Bourse French Tech Emergence program. J.D. would also like to gratefully acknowledge Institut Universitaire de France (IUF) for financial support.

Appendix A. Supplementary material

Supplementary material related to this article can be found online at https://doi.org/10.1016/j.matdes.2024.113553.

Data availability

Data will be made available on request.

References

[1] M.F. Ashby, Y. Bréchet, Designing hybrid materials, Acta Mater. 51 (2003) 5801–5821.
[2] O. Bouaziz, Y. Bréchet, J.D. Embury, Heterogeneous and architectured materials: a possible strategy for design of structural materials, Adv. Eng. Mater. 10 (1–2) (2008) 24–36, https://doi.org/10.1002/adem.200700289.
[3] Y. Bréchet, J.D. Embury, Architectured materials: expanding materials space, Scr. Mater. 68 (1) (2013) 1–3.
[4] J.C. Maxwell, On the calculation of the equilibrium and stiffness of frames, Lond. Edinb. Dublin Philos. Mag. J. Sci. 27 (182) (1864) 294–299.
[5] I. Gibson, M.F. Ashby, The mechanics of three-dimensional cellular materials, Proc. R. Soc. Lond. Ser. A, Math. Phys. Sci. 382 (1782) (1982) 43–59.
[6] M.F. Ashby, The properties of foams and lattices, Philos. Trans. R. Soc. A, Math. Phys. Eng. Sci. 364 (1838) (2006) 15–30.
[7] V.S. Deshpande, N.A. Fleck, M.F. Ashby, Effective properties of the octet-truss lattice material, J. Mech. Phys. Solids 49 (8) (2001) 1747–1769.
[8] N.A. Fleck, V.S. Deshpande, M.F. Ashby, Micro-architectured materials: past, present and future, Proc. R. Soc. A, Math. Phys. Eng. Sci. 466 (2121) (2010) 2495–2516.
[9] D. Rayneau-Kirkhope, Y. Mao, R. Farr, Ultralight fractal structures from hollow tubes, Phys. Rev. Lett. 109 (2012) 204301.
[10] A. Vigliotti, D. Pasini, Stiffness and strength of tridimensional periodic lattices, Comput. Methods Appl. Mech. Eng. 229 (2012) 27–43.
[11] T.P. Hughes, A. Marmier, K.E. Evans, Auxetic frameworks inspired by cubic crystals, Int. J. Solids Struct. 47 (2010) 1469–1476.
[12] J. Dirrenberger, S. Forest, D. Jeulin, Effective elastic properties of auxetic microstructures: anisotropy and structural applications, Int. J. Mech. Mater. Des. 9 (1) (2013) 21–33, https://doi.org/10.1007/s10999-012-9192-8.
[13] G. Rosi, N. Auffray, Anisotropic and dispersive wave propagation within strain-gradient framework, Wave Motion 63 (2016) 120–134.
[14] G. Rosi, N. Auffray, Continuum modelling of frequency dependent acoustic beam focussing and steering in hexagonal lattices, Eur. J. Mech. A, Solids 77 (2019) 103803, https://doi.org/10.1016/j.euromechsol.2019.103803.
[15] A. Álvarez Trejo, E. Cuan-Urquizo, D. Bhate, A. Roman-Flores, Mechanical metamaterials with topologies based on curved elements: an overview of design, additive manufacturing and mechanical properties, Mater. Des. 233 (2023) 112190, https://doi.org/10.1016/j.matdes.2023.112190.
[16] X. Li, M. Zhao, X. Yu, J. Wei Chua, Y. Yang, K.M. Lim, W. Zhai, Multifunctional and customizable lattice structures for simultaneous sound insulation and structural applications, Mater. Des. 234 (2023) 112354, https://doi.org/10.1016/j.matdes.2023.112354.

[17] A. Ciallella, I. Giorgio, E. Barchiesi, G. Alaimo, A. Cattenone, B. Smaniotto, A. Vintache, F. D'Annibale, F. dell'Isola, F. Hild, F. Auricchio, A 3D pantographic metamaterial behaving as a mechanical shield: experimental and numerical evidence, Mater. Des. 237 (2024) 112554, https://doi.org/10.1016/j.matdes.2023.112554.

[18] Y. Bao, Z. Wei, Z. Jia, D. Wang, X. Zhang, Z. Kang, Mechanical metamaterial design with the customized low-frequency bandgap and negative Poisson's ratio via topology optimization, Extrem. Mech. Lett. 67 (2024) 102124, https://doi.org/10.1016/j.eml.2024.102124.

[19] X. Li, J.W. Chua, X. Yu, Z. Li, M. Zhao, Z. Wang, W. Zhai, 3D-printed lattice structures for sound absorption: current progress, mechanisms and models, structural-property relationships, and future outlook, Adv. Sci. 11 (4) (2024) 2305232, https://doi.org/10.1002/advs.202305232.

[20] T.A. Schaedler, A.J. Jacobsen, A. Torrents, A.E. Sorensen, J. Lian, J.R. Greer, L. Valdevit, W.B. Carter, Ultralight metallic microlattices, Science 334 (6058) (2011) 962–965.

[21] T. Tancogne-Dejean, A.B. Spierings, D. Mohr, Additively-manufactured metallic micro-lattice materials for high specific energy absorption under static and dynamic loading, Acta Mater. 116 (2016) 14–28, https://doi.org/10.1016/j.actamat.2016.05.054.

[22] C. de Formanoir, M. Suard, R. Dendievel, G. Martin, S. Godet, Improving the mechanical efficiency of electron beam melted titanium lattice structures by chemical etching, Addit. Manuf. 11 (2016) 71–76.

[23] F. Albertini, J. Dirrenberger, C. Sollogoub, T. Maconachie, M. Leary, A. Molotnikov, Experimental and computational analysis of the mechanical properties of composite auxetic lattice structures, Addit. Manuf. 47 (2021) 102351.

[24] S. Ford, M. Despeisse, Additive manufacturing and sustainability: an exploratory study of the advantages and challenges, J. Clean. Prod. 137 (2016) 1573–1587, https://doi.org/10.1016/j.jclepro.2016.04.150.

[25] M. Baumers, P. Dickens, C. Tuck, R. Hague, The cost of additive manufacturing: machine productivity, economies of scale and technology-push, Technol. Forecast. Soc. Change 102 (2016) 193–201, https://doi.org/10.1016/j.techfore.2015.02.015.

[26] J. Teubler, S. Weber, P. Suski, I. Peschke, C. Liedtke, Critical evaluation of the material characteristics and environmental potential of laser beam melting processes for the additive manufacturing of metallic components, J. Clean. Prod. 237 (2019) 117775, https://doi.org/10.1016/j.jclepro.2019.117775.

[27] J.J. Heinen, K. Hoberg, Assessing the potential of additive manufacturing for the provision of spare parts, J. Oper. Manag. 65 (8) (2019) 810–826, https://doi.org/10.1002/joom.1054.

[28] M. Sauerwein, E. Doubrovski, R. Balkenende, C. Bakker, Exploring the potential of additive manufacturing for product design in a circular economy, J. Clean. Prod. 226 (2019) 1138–1149, https://doi.org/10.1016/j.jclepro.2019.04.108.

[29] H.H. Shah, C. Tregambi, P. Bareschino, F. Pepe, Environmental and economic sustainability of additive manufacturing: a systematic literature review, Sustain. Prod. Consump. (2024).

[30] M.R.K. Ravari, S.N. Esfahani, M.T. Andani, M. Kadkhodaei, A. Ghaei, H. Karaca, M. Elahinia, On the effects of geometry, defects, and material asymmetry on the mechanical response of shape memory alloy cellular lattice structures, Smart Mater. Struct. 25 (2) (2016) 025008, https://doi.org/10.1088/0964-1726/25/2/025008, publisher: IOP Publishing.

[31] A. Großmann, J. Gosmann, C. Mittelstedt, Lightweight lattice structures in selective laser melting: design, fabrication and mechanical properties, Mater. Sci. Eng. A 766 (2019) 138356, https://doi.org/10.1016/j.msea.2019.138356.

[32] A. Alghamdi, D. Downing, R. Tino, A. Almalki, T. Maconachie, B. Lozanovski, M. Brandt, M. Qian, M. Leary, Buckling phenomena in AM lattice strut elements: a design tool applied to Ti-6Al-4V LB-PBF, Mater. Des. 208 (2021) 109892, https://doi.org/10.1016/j.matdes.2021.109892.

[33] E. Maleki, S. Bagherifard, M. Bandini, M. Guagliano, Surface post-treatments for metal additive manufacturing: progress, challenges, and opportunities, Addit. Manuf. 37 (2021) 101619, https://doi.org/10.1016/j.addma.2020.101619.

[34] D. Thomas, Costs, benefits, and adoption of additive manufacturing: a supply chain perspective, Int. J. Adv. Manuf. Technol. 85 (5) (2016) 1857–1876, https://doi.org/10.1007/s00170-015-7973-6.

[35] R. Paul, S. Anand, F. Gerner, Effect of thermal deformation on part errors in metal powder based additive manufacturing processes, J. Manuf. Sci. Eng. 136 (Mar. 2014) 031009, https://doi.org/10.1115/1.4026524.

[36] I. Echeta, X. Feng, B. Dutton, R. Leach, S. Piano, Review of defects in lattice structures manufactured by powder bed fusion, Int. J. Adv. Manuf. Technol. 106 (5) (2020) 2649–2668, https://doi.org/10.1007/s00170-019-04753-4.

[37] S.-g. Chen, H.-j. Gao, Y.-d. Zhang, Q. Wu, Z.-h. Gao, X. Zhou, Review on residual stresses in metal additive manufacturing: formation mechanisms, parameter dependencies, prediction and control approaches, J. Mater. Res. Technol. 17 (2022) 2950–2974, https://doi.org/10.1016/j.jmrt.2022.02.054.

[38] M.A. Matos, A.M.A.C. Rocha, A.I. Pereira, Improving additive manufacturing performance by build orientation optimization, Int. J. Adv. Manuf. Technol. 107 (5) (2020) 1993–2005, https://doi.org/10.1007/s00170-020-04942-6.

[39] T. de Terris, O. Andreau, P. Peyre, F. Adamski, I. Koutiri, C. Gorny, C. Dupuy, Optimization and comparison of porosity rate measurement methods of Selective Laser Melted metallic parts, Addit. Manuf. 28 (2019) 802–813, https://doi.org/10.1016/j.addma.2019.05.035.

[40] W.H. Kan, L.N.S. Chiu, C.V.S. Lim, Y. Zhu, Y. Tian, D. Jiang, A. Huang, A critical review on the effects of process-induced porosity on the mechanical properties of alloys fabricated by laser powder bed fusion, J. Mater. Sci. 57 (21) (2022) 9818–9865, https://doi.org/10.1007/s10853-022-06990-7.

[41] N. Ravi, V. Gabeur, Y.-T. Hu, R. Hu, C. Ryali, T. Ma, H. Khedr, R. Rädle, C. Rolland, L. Gustafson, et al., Sam 2: segment anything in images and videos, arXiv preprint, arXiv:2408.00714, 2024.

[42] H. Assimi, A. Jamali, N. Nariman-Zadeh, Multi-objective sizing and topology optimization of truss structures using genetic programming based on a new adaptive mutant operator, Neural Comput. Appl. 31 (10) (2019) 5729–5749.

[43] N. Panagant, N. Pholdee, S. Bureerat, A.R. Yildiz, S. Mirjalili, A comparative study of recent multi-objective metaheuristics for solving constrained truss optimisation problems, Arch. Comput. Methods Eng. (2021) 1–17.

[44] P.M.d.O. Silva, H.F.G. de Abreu, V.H.C. de Albuquerque, P. de Lima Neto, J.M.R. Tavares, Cold deformation effect on the microstructures and mechanical properties of aisi 301ln and 316l stainless steels, Mater. Des. 32 (2) (2011) 605–614.

[45] D. Özyürek, An effect of weld current and weld atmosphere on the resistance spot weldability of 304l austenitic stainless steel, Mater. Des. 29 (3) (2008) 597–603.

[46] D. Kianersi, A. Mostafaei, A.A. Amadeh, Resistance spot welding joints of aisi 316l austenitic stainless steel sheets: phase transformations, mechanical properties and microstructure characterizations, Mater. Des. 61 (2014) 251–263.

[47] Préparation métallographique de l'acier inoxydable, https://www.struers.com/-/media/Library/Brochures/French/Preparation-metallographique-de-l-acier-inoxydable.pdf.

[48] Suyitno, B. Arifvianto, T.D. Widodo, M. Mahardika, P. Dewo, U.A. Salim, Effect of cold working and sandblasting on the microhardness, tensile strength and corrosion resistance of aisi 316l stainless steel, Int. J. Miner. Metal. Mater. 19 (2012) 1093–1099.

[49] K.-T. Kim, Mechanical performance of additively manufactured austenitic 316l stainless steel, Nucl. Eng. Technol. 54 (1) (2022) 244–254.